(Al,In)N layers and (Al,In)N/GaN heterostructures grown by plasma-assisted molecular beam epitaxy on 6*H*-SiC(0001)

Tommy Ive,* Oliver Brandt, Xiang Kong,† Achim Trampert, and Klaus H. Ploog
Paul-Drude-Institut für Festkörperelektronik, Hausvogteiplatz 5-7, D-10117 Berlin, Germany
(Received 23 March 2008; published 10 July 2008)

We study the properties of (Al,In)N layers and (Al,In)N/GaN heterostructures grown on 6*H*-SiC(0001) by plasma-assisted molecular beam epitaxy. The (Al,In)N films are deposited on a GaN buffer layer. A growth temperature of 500 °C and above results in low In contents which give rise to cracks due to the large tensile strain experienced from the underlying GaN buffer layer. In addition, these layers exhibit strong phase separation leading to inhomogeneous In composition and rough surfaces. In contrast, samples with homogeneous and well-controlled In-contents between 10%–30% are reproducibly obtained in the temperature range of 250–350 °C. Surprisingly, nominally lattice-matched layers with an In content of 17%–18% also exhibit cracks. Symmetric $\omega-2\theta$ x-ray diffraction scans and reciprocal space maps reveal the presence of a strain gradient in these layers despite the apparently lattice-matched conditions. Transmission electron microscopy indicates that these cracks are the result of tensile stresses induced by crystallite coalescence and grain-boundary formation. This mechanism can be counteracted by augmenting the adatom mobility through increasing the growth temperature and the N flux. However, phase separation sets an upper limit on the growth temperature and a moderate increase to 350–400 °C is sufficient to obtain crack-free and homogeneous (Al,In)N layers. The results of our growth experiments lead to a phase diagram which shows the optimum growth window for (Al,In)N layers. By choosing the growth conditions within this window, we are able to obtain crack-free $Al_{0.82}In_{0.18}N/GaN$ multilayers with abrupt interfaces.

DOI: 10.1103/PhysRevB.78.035311 PACS number(s): 68.55.Nq, 78.66.Fd, 81.15.Hi

I. INTRODUCTION

Nitride-based materials have become the cornerstone for the production of light emitting diodes (LEDs) and laser diodes emitting in the blue-violet wavelength range. These devices are based on heterostructures made of (In,Ga)N and (Al,Ga)N compounds. The large lattice mismatch between (In,Ga)N and (Al,Ga)N inevitably lead to the formation of defects at the interfaces between the different compounds. Defects have a detrimental impact on the electrical and optical properties of the materials. The situation is worsened by the lack of commercially available single-crystal nitride substrates. In addition, careful strain management is needed in order to avoid strain related effects and crack formation. Interestingly, epitaxial (Al,In)N films containing 18% In are lattice matched to GaN. Despite this highly desirable property there exist only a few reports on the growth of this material system. The reason is that the large miscibility gap between AlN and InN makes the growth of this ternary compound very difficult. It is well-known that (In,Ga)N is prone to spinodal decomposition due to the large miscibility gap between InN and GaN.[1] This tendency is even more pronounced for (Al,In)N. In fact, it has been predicted[2] that in the group InN–GaN, AlN–GaN, and AlN–InN the largest miscibility gap occurs for (Al,In)N.

Recently, using metal-organic chemical vapor deposition (MOCVD), successful growth of both crack-free Bragg reflectors of high reflectance and fully epitaxially grown microcavities with a Q factor of 800 have been demonstrated by Carlin and Dorsaz and coworkers.[3–6] It should be noted that Bragg reflectors based on other nitride compounds such as (Al,Ga)N are notoriously difficult to synthesize due to crack formation caused by the strain accumulation that is induced by the large lattice mismatch between the materials. An immediate application of lattice matched and therefore crack-free $Al_{0.82}In_{0.18}N/GaN$ Bragg reflectors would be to enhance the light extraction of short-wavelength LEDs by introducing a resonant-cavity structure into the LEDs. It has been predicted that (Al,In)N/GaN heterostructures possess very favorable properties for field-effect transistors (FETs).[7] A number of groups have grown (Al,In)N/GaN FET structures employing MOCVD (Refs. 8 and 9) and plasma-assisted molecular beam epitaxy (PAMBE).[10] (Al,In)N has also been grown by sputtering techniques.[11,12] However, to this date, there are no comprehensive reports focused on the details of the growth of (Al,In)N layers and heterostructures.

In this work, we present a study on the growth and properties of (Al,In)N layers grown by PAMBE on 6*H*-SiC(0001). The corresponding PAMBE growth conditions for AlN and InN are very different. High-quality AlN layers are obtained at a high growth temperature (>800 °C) and under Al-stable conditions.[13] For In-face InN, a low growth temperature is required since InN decomposes at 500–550 °C.[14] In addition, In-stable growth conditions lead to layers containing metallic In inclusions.[14] Based on the results of our (Al,In)N growth experiments, we could construct a phase diagram from which we identified an optimum growth window for (Al,In)N. Using the growth conditions derived from this growth window we were able to grow smooth and crack-free (Al,In)N layers with a homogeneous In content. Choosing the same optimum conditions we also synthesized $Al_{0.82}In_{0.18}N/GaN$ multilayers.

A combination of transmission electron microscopy (TEM), x-ray diffraction (XRD), atomic force microscopy (AFM), and differential interference-contrast (DIC) optical microscopy revealed that crack formation can occur in spite

of apparently lattice-matched conditions. The cause of this crack formation is crystallite coalescence and grain-boundary formation as proposed by Nix and Clemens.[15]

II. EXPERIMENT

The growth experiments were conducted in a custom-built three-chamber molecular beam epitaxy (MBE) system made by Createc™. The system is equipped with solid source effusion cells for Al, Ga, and In, a water-cooled rf nitrogen plasma source (SVTA™) for producing active N, and a reflectance high-energy electron diffraction (RHEED) gun operated at 20 keV for monitoring the growth front. The system has a base pressure of 5×10^{-11} Torr. We use 6N N_2 gas as a precursor which is further purified to 5 ppb by a getter filter. All samples are continuously rotated during growth.

Conducting *n*-type (10^{-3} Ω cm) 6*H*-SiC(0001) epi-ready wafers (produced by Cree™ and polished by NovaSiC™) are used as substrates. The mounting procedure is performed in ambient and therefore suboxides form on the SiC surface. These suboxides are effectively removed by an *in situ* Ga-polishing or Ga flash-off procedure.[16] It is well-known that the bare SiC surface prior to the Ga flash-off procedure produces a 1×1 RHEED pattern. An abrupt transition from the 1×1 RHEED pattern to a sharp 3×1 RHEED pattern is observed once the surface is free of suboxides. This 3×1 RHEED pattern occurs at 720 °C and corresponds to a Si-induced surface reconstruction.[17] The transition was used as an *in situ* temperature calibration of the substrate temperature before each individual growth run. Occasionally, as independent calibration methods, the temperature is calibrated by pyrometry and visual observation of the melting point of Al (660 °C). In the latter case, the Al is deposited at a growth temperature which is below its melting point. The Al layer grows in a crystalline manner and thus it gives rise to a distinct transmission RHEED pattern. The temperature is increased and once it reaches the melting point of Al the film melts and the RHEED pattern disappears reflecting the amorphous state of the Al melt. The same procedure has been performed with In, which melts at 157 °C, thus serving as a low-temperature calibration point.

GaN buffer layers were grown on 6*H*-SiC substrates at 750 °C under Ga-stable conditions which yield excellent results in terms of surface morphology, crystal quality, and electrical and optical properties.[16,18–20] Using these Ga-stable conditions, the desorption and the absorption of Ga on the growing surface balance each other thereby forming a Ga bilayer on the surface. The bilayer is stable under steady-state conditions and promotes the mobility of the Ga adatoms yielding very smooth films. The operating power of the nitrogen plasma source was 300 W and the N_2 flux was set to 1 cubic centimeter per minute at standard temperature and pressure (sccm). These conditions gave a GaN growth rate of 400–450 nm/h. All samples have a buffer layer thickness of 200–225 nm. A streaky 1×1 RHEED pattern during the entire GaN growth run evidenced two-dimensional growth and a smooth surface. The structural properties of these GaN buffer layers are described in detail in Ref. 21.

A Zeiss Axiotech™ DIC optical microscope with a maximum magnification of 1000× and fitted with a charge coupled device camera was used to determine the presence of droplets or remnants of droplets ("footprints"), crystallites, and cracks on the sample surface. AFM scans were performed with a Veeco Dimension 3100™ atomic force microscope. The instrument was operated in tapping mode with a Si cantilever. All AFM measurements were done under ambient conditions. XRD measurements were performed with a Philips X'Pert PRO™ four-circle triple-axis diffractometer equipped with a $Cu_{K\alpha_1}$ ($\lambda=0.154\ 056\ 2$ nm) source in the focus of a multilayer x-ray mirror and a Ge(022) hybrid monochromator. Symmetric ω-2θ XRD measurements for the (Al,In)N(0002) reflection were used to determine the In content and the film thickness. We used XRD reciprocal space maps (RSM) to determine the strain state of the samples. The polar and azimuthal orientational spread (tilt and twist) was examined by recording x-ray rocking curves across the symmetric (0002) reflection and in skew geometry across the $(10\bar{1}2)$ reflection, respectively. A JEOL 3010™ TEM microscope operating at 300 kV was used to obtain the TEM micrographs. Electron energy-loss spectroscopy (EELS) gave information about the layers' local composition. For reflectance measurements, a Filmetrics F20™ reflectometer was employed.

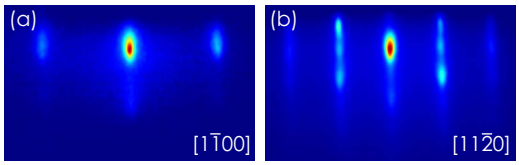

FIG. 1. (Color online) Representative RHEED pattern observed for (Al,In)N layers after 2–3 min of N-rich growth on GaN.

III. RESULTS

A. Nucleation and growth front

All (Al,In)N layers nucleated two-dimensionally on the GaN buffer layer as evidenced by an initially streaky RHEED pattern. The layers were grown under N-rich conditions. After 2–3 min of growth (layer thickness=10 nm) a transition from a perfectly streaky RHEED pattern to a pattern with streaks having an undulated shape (modulated streaks), as shown in Fig. 1, occurred. From this point on, the RHEED pattern remained essentially unchanged throughout the growth. At the end of a growth run, the pattern was usually slightly faceted with a facet angle of not more than 5°.

B. High temperature range—type I cracks

The employed growth parameters and the results of our growth experiments are summarized in Fig. 2 which shows the MBE phase diagram deduced from 100–500 nm thick (Al,In)N layers with an In content varying between 10%–30% grown at a rate of 200 nm/h [higher growth rates (400 nm/h) shifts the entire phase diagram rigidly upwards, but gave generally poorer results]. Homogeneous and crack-free samples were obtained only by choosing the growth parameters from the shaded area, as detailed below.

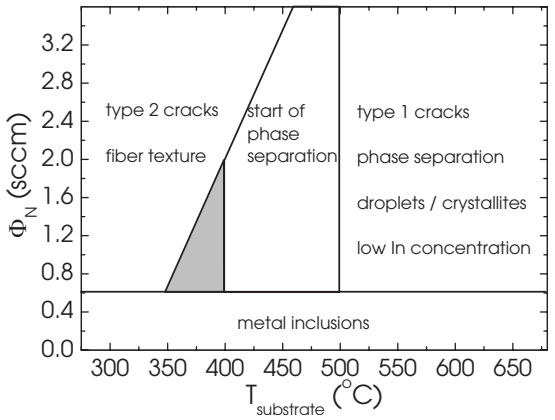

FIG. 2. MBE phase diagram of 100–500 nm thick (Al,In)N layers. The In content is 10%–30% in all regions except in the type 1 crack region which has an In content of <8% region and in the region where metallic In inclusions are observed. All layers were grown on a GaN buffer layer under N-rich conditions. Homogeneous and crack-free samples were obtained only by choosing growth conditions from the shaded area.

The onset of phase separation lies in the 400–500 °C region. All layers were grown on a GaN buffer layer. At a temperature higher than 500 °C, the segregated InN starts to decompose leaving In droplets on the surface. It becomes increasingly more difficult to reach an In content of 17%–18% which is required for lattice-matched conditions. Practically no In is incorporated at a temperature of 600 °C or above. The low In content leads to crack formation (type 1 cracks) due to the tensile strain that the layer experiences from the underlying GaN buffer layer. It should be noted that (In,Ga)N layers of excellent quality were grown by our group at this growth temperature (600 °C).[22]

Figure 3 shows a DIC optical micrograph of a 160 nm thick (Al,In)N sample grown at 660 °C under extremely N-rich conditions (N flux=3 sccm). In droplets of varying size can be observed despite the extremely N-rich growth conditions. Following the discussion above, these In droplets are the result of phase-segregated InN that has decomposed. The epitaxial film has thus a very low In content (Fig. 4) and is therefore under a high tensile strain due to the GaN buffer. This is the reason for the massive crack formation that is observed in Fig. 3.

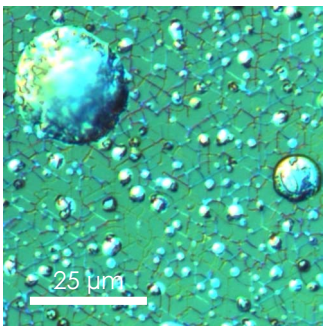

FIG. 3. (Color online) DIC optical micrograph of a sample grown at 660 °C under extremely N-rich conditions on a GaN buffer layer. In droplets of varying size and a network of cracks are visible.

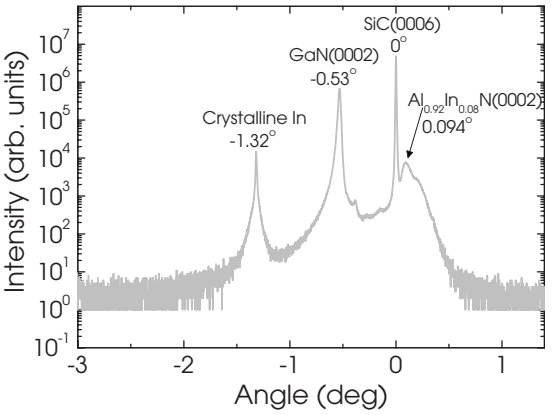

FIG. 4. XRD ω-2θ scan across the GaN(0002) reflection of the sample grown at 660 °C under extremely N-rich conditions on a GaN buffer layer. A weak and broad $Al_{0.92}In_{0.08}N$ reflection is visible very close to SiC(0006). Crystalline In contained in either droplets or inclusions cause the reflection just left of GaN(0002). All positions are relative to the SiC(0006) reflection.

Figure 4 shows an ω-2θ XRD scan for the (Al,In)N(0002) reflection of the sample which was grown at 660 °C. A weak and broad $Al_{0.92}In_{0.08}N$ reflection can be observed. The low In-content layer experiences a large tensile strain from the underlying GaN buffer layer. The result is a massive crack formation as observed in Fig. 3. We can also see a crystalline In-related reflection [−1.32° relative to SiC(0006)] which is the consequence of phase segregation (Fig. 3). The cause of this In reflection is that temperature is high enough to decompose InN but not high enough to desorb the remaining In residing on the surface. Under ambient conditions, In is crystalline and therefore gives rise to an In-related XRD reflection.

A cross-sectional TEM micrograph of a sample grown at 600 °C is shown in Fig. 5. Phase separation can be observed in the form of 0.5–0.6 μm wide In-rich polycrystalline remnants of In droplets.

The region between the droplets has a low and laterally very inhomogeneous In content (6%–14%), as revealed by EELS measurements.

C. Low-temperature range—type 2 cracks

In order to avoid type 1 cracks and droplets, we drastically lowered the growth temperature down to 300–375 °C.

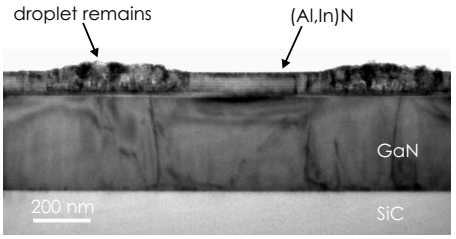

FIG. 5. Cross-sectional TEM micrograph of a sample grown at 600 °C. Large In-rich polycrystalline In-droplet remnants are observed. The layer between the droplets has a low and very inhomogeneous In content.

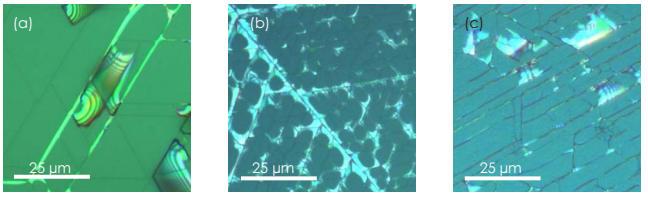

FIG. 6. (Color online) DIC optical micrographs of the surfaces of three samples grown at (a) 375 °C and [(b) and (c)] 300 °C. The In contents are 26.6% in (a) and 18.5 and 17.5% in (b) and (c), respectively. A network of cracks is clearly visible for all samples. Regions where the epitaxial film has completely detached from the substrate surface give rise to the optical interference fringes visible particularly well in (a).

This action inhibits phase separation and increases the In content in the (Al,In)N layers. As mentioned, the effect of the low In-content in the samples grown at high temperatures is that the underlying GaN buffer layer induces a high tensile strain in the low In-content (Al,In)N layer. The high tensile strain leads to crack formation.

Our samples grown in the 300–375 °C range have an In content between 11% and 27%. The low growth temperature allows a good control of the In incorporation and we therefore reproducibly obtain the desired In content of 18% required for lattice matching.

Figure 6 shows DIC optical micrographs of the surfaces of three samples grown at 375 °C (a) and 300 °C [(b) and (c)]. We used a N flux of 2.0 sccm for all samples which are 140–200 nm thick. The In content is 26.6% in (a) and 18.5 and 17.5%, respectively, in (b) and (c). The sample in (a) should be under a strong compressive strain whereas the samples in (b) and (c) should be very close to lattice-matched conditions. We see that the surface morphology is similar in all cases. A dense network of hairline cracks and less dense large cracks are visible in all samples. We also observe regions where the epitaxial film has detached completely from the substrate surface. These very thin free standing regions give rise to the optical interference fringes visible particularly well in (a).

Essentially, all films grown under similar low-temperature conditions as the samples shown in Fig. 6 and with the In content of 18% exhibit cracks. This is very surprising because layers under a slight compressive strain ($0.20 > x_{\mathrm{In}} > 0.18$) or under lattice-matched conditions ($x_{\mathrm{In}}=0.18$) should in principle not show any cracks. For this reason we denote this type of cracks as type 2 cracks emphasizing that their origin is different from that of the type 1 cracks. Note that, as described earlier, the RHEED pattern remains essentially unchanged after the first 2–3 min of growth. This indicates that the cracks form during the earliest phase of the growth run.

Figure 7 shows an ω-2θ XRD measurement across the (Al,In)N(0002) reflection that is typical for all low-temperature grown samples. The gray curve in Fig. 7(a) represents the experimental data from a 126 nm thick $Al_{0.73}In_{0.27}N$ layer and the black curve represents a fit to the experimental data. We see that we can fit both the peak positions and the widths correctly. The simulated interference fringes, though, have an intensity that is too low. We see also

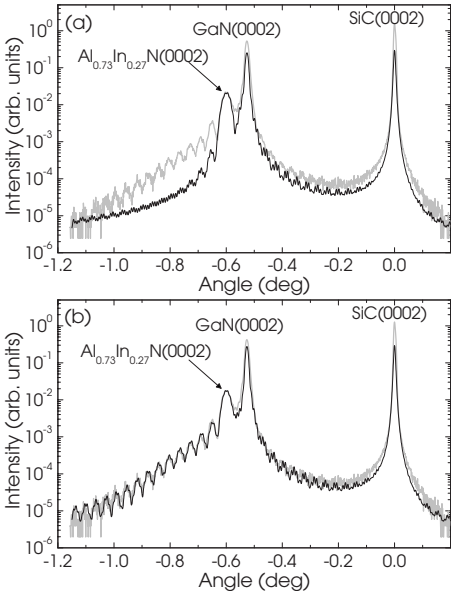

FIG. 7. XRD ω-2θ scan across the (Al,In)N(0002) reflection for a sample representative of all low-temperature grown layers. The experimental data is represented by the gray line and the fit is represented by the black line. In (a) the fit is done without a strain gradient. In (b) a strain gradient is included yielding an almost perfect fit.

that the shape of the simulated curve is different. An acceptable fit can only be achieved by including a strain gradient [Fig. 7(b)]. Here, we assume that the layer is experiencing a progressively larger tensile strain evolving 20 nm into the layer from the GaN/$Al_{0.73}In_{0.27}N$ interface. At a first glance, this is expected since an In content of 27% yields an in-plane lattice constant a that is larger than that of GaN and therefore the layer relaxes. However, the same behavior is observed even for samples that have the desired In content of 17%–18% which is required for the layers to be lattice matched to GaN. It should be emphasized that for these apparently lattice-matched samples we have to assume that the strain gradient is evolving from a strain-free lattice-matched state at the GaN/(Al,In)N interface to a gradually larger tensile strain. This is a seemingly paradoxical assumption because there is, at first glance, no reason for a layer that is lattice matched to the buffer layer to be under tensile strain. Nevertheless, the RSM displayed in Fig. 8 unambiguously shows that this is indeed the case.

Figure 8 depicts a RSM obtained from a 170 nm thick (Al,In)N layer with an In content of 17%. It is therefore nearly lattice matched to GaN. The contour plot shows that there are two reflections related to the (Al,In)N layer. One of these reflections [coherent (Al,In)N in Fig. 8] is on the same horizontal position (white dashed line in Fig. 8) as that related to the GaN buffer layer. Because a shift in the horizontal position in a RSM corresponds to a shift of the in-plane lattice constant a we can conclude that the part of the (Al,In)N layer closest to the GaN buffer layer has the same a as GaN. It is thus coherent to the underlying GaN buffer layer. The second reflection [strained (Al,In)N in Fig. 8] lies to the left of the GaN reflection which means that the a value is larger than that of GaN. We can immediately compare the

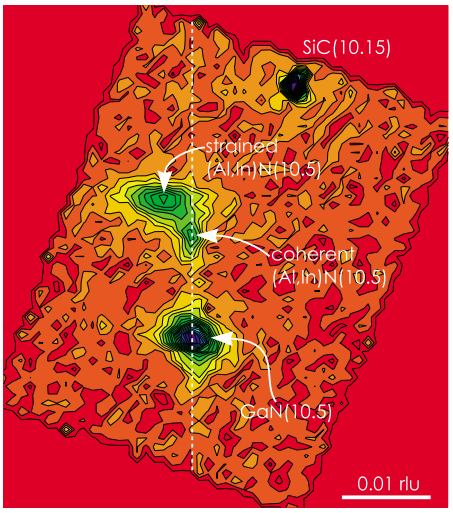

FIG. 8. (Color online) Reciprocal space map of a 170 nm thick $Al_{0.83}In_{0.17}N$ layer grown at 300 °C with a N flux of 2 sccm. Indicated are the reflections corresponding to the SiC substrate, the GaN buffer layer, and the coherent and strained $Al_{0.83}In_{0.17}N$.

in- a and out-of-plane c lattice constants for the two (Al,In)N reflections because a vertical shift in a RSM directly corresponds to a shift of c. The in- and out-of-plane lattice constants are related through Poisson's relations and Vegard's law. The results calculated from these relations should be fairly consistent with the results from the RSM. However, when using Vegard's law, both with and without bowing,[23] and Poisson's relations, a large discrepancy is found when compared to the results from the RSM.

We examined our low-temperature grown samples by TEM in order to better understand the apparently contradicting XRD results. Figure 9 shows a cross-sectional TEM micrograph of a 145 nm thick $Al_{0.79}In_{0.21}N$ sample grown at 300 °C with an N flux of 2.0 sccm. No phase separation can be observed. In addition, EELS measurements, an example of which is shown in Fig. 10, show that In has been incorporated homogeneously in the layer. TEM micrographs taken with $\mathbf{g}=1\bar{1}00$ as shown in Fig. 11 reveal that the layer exhibits columnar growth as in the case of the high-temperature sample. However, here the width of the columns is much smaller (≈20 nm). Skew geometry XRD measurements reveal that the columns have a small tilt but a large twist (2°). High-resolution TEM micrographs of samples with an In content of 16%–18% show, as expected, that no misfit dislocations exist at the (Al,In)N/GaN interface. Despite of this indication for lattice matching, the layer exhibits cracks as indicated by the black arrows in Fig. 9.

Based on the results from the XRD and TEM measurements, it will be shown in the following that the formation of

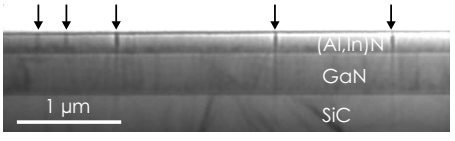

FIG. 9. Cross-sectional TEM micrograph of a 145 nm thick $Al_{0.793}In_{0.207}N$ sample grown at 300 °C with a N flux of 2.0 sccm. The black arrows indicate cracks in the layer.

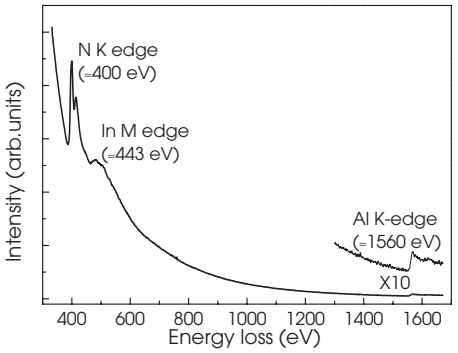

FIG. 10. EELS spectrum of a 145 nm thick $Al_{0.793}In_{0.207}N$ sample grown at 300 °C with a N flux of 2.0 sccm.

type 2 cracks can be explained by tensile stresses induced by crystallite coalescence and grain-boundary formation as proposed by Nix and Clemens.[15]

The low growth temperature and the high N flux results in a nanocolumnar growth of (Al,In)N [Fig. 12(a)]. These ≈20 nm wide crystallites/columns have a small tilt but a considerable twist of ≈2°. Columns with an In content of 16%–18% initially grow coherently ($a_{GaN}=a_{(Al,In)N}$) on the GaN buffer layer. This means that there are no misfit dislocations at the GaN/(Al,In)N interface, as demonstrated by TEM. As the growth progresses, the column surfaces spontaneously start "snapping" together [Fig. 12(b)] thereby forcing the columns to coalesce and to form [0001] tilt grain boundaries. This occurs since the free energy of the formed grain boundaries is lower than the free energy needed for sustaining free column surfaces.

Following Nix and Clemens,[15] the average tensile stress σ_{avg} generated by the coalescence process can be estimated by

$$\sigma_{avg} = \left[\left(\frac{1+\nu}{1-\nu} \right) Y \frac{(2\gamma_{sv} - \gamma_{gb})}{a} \right]^{1/2}, \quad (1)$$

where Y, ν, and a represent Young's modulus, Poisson's ratio, and crystallite size [as shown in Fig. 12(a)], respectively. The free energy of the crystallites surface and the grain boundaries are denoted by γ_{sv} and γ_{gb}, respectively.

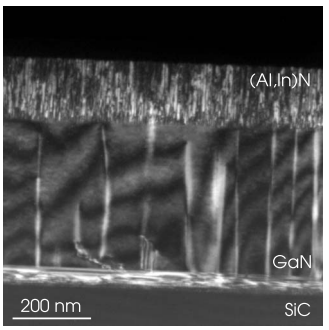

FIG. 11. Cross-sectional TEM micrograph with $\mathbf{g}=1\bar{1}00$ of a 145 nm thick $Al_{0.83}In_{0.17}N$ sample grown at 350 °C with a N flux of 2.0 sccm. The diffraction conditions are chosen to be sensitive to dislocations with edge character.

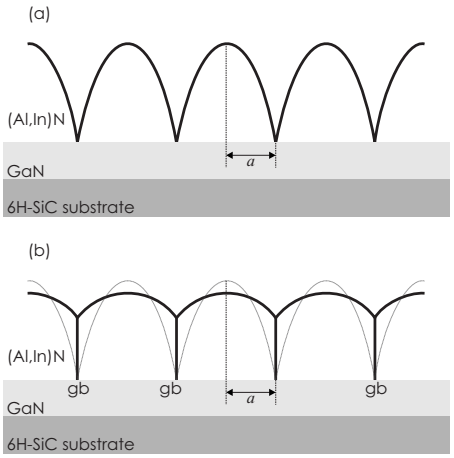

FIG. 12. Crystallite coalescence and grain-boundary formation process (after Ref. 15). The initial stages of the growth is shown in (a). Here, the (Al,In)N crystallites and/or columns grow separately on the GaN buffer layer. In (b) crystallite coalescence has occurred forming a continuous film which is under tensile strain.

A column, which coalesces with surrounding columns, faces a largely biaxial stress acting in the growth plane. This situation is analogous to the in-plane stress due to epitaxial growth of mismatched layers. In this case, the Poisson ratio is given by

$$\nu = -\frac{\varepsilon_{\perp}}{\varepsilon_{\parallel}} = 2\frac{C_{13}}{C_{33}}, \tag{2}$$

and the Young modulus by

$$Y = C_{11} + C_{12} - 2\frac{C_{13}^2}{C_{33}}. \tag{3}$$

Here, $\varepsilon_{\perp}$ and $\varepsilon_{\parallel}$ denote the out-of-plane and in-plane strain components and the C_{ij} are components of the stiffness tensor. Using the stiffness constants for AlN calculated in Ref. 24, we arrive at $\nu=0.368$ and $Y=511$ GPa.

To the best of our knowledge, values for the surface and grain-boundary energies are not available for AlN or InN. For GaN, however, the surface energy of the $(10\bar{1}0)$ prism plane (the side face of the columns) has been calculated to be 1.76 J/m^2.[25] Furthermore, the energy of [0001] tilt grain boundaries in GaN has been calculated in Ref. 26. For small angles, the computed energies γ_{gb} have been shown to follow isotropic elasticity theory:

$$\gamma_{gb} = E_0\theta\{(\pi R\theta/b)\coth(\pi R\theta/b) - \ln[2\sinh(\pi R\theta/b)]\}, \tag{4}$$

with $E_0=3.55$ J/m^2 and $R=0.6b$, where b is the magnitude of the Burgers vector.[26] For a tilt angle θ equal to the measured twist between the columns (i.e., $\theta=2°$), this equation predicts $\gamma_{gb}=0.375$ J/m^2. Finally, the crystallite and/or column dimension is $2a=40$ nm as revealed by TEM.

Using Eq. (1) and the values given above, we obtain $\sigma_{avg}=13.2$ GPa. This considerable stress is comparable to the in-plane stress $\sigma_{\parallel}$ experienced by a thin AlN epitaxial layer grown on GaN ($\sigma_{\parallel}=Y\varepsilon_{\parallel}=12.6$ GPa). Note that AlN, when exceeding a thickness of about 20 nm, cracks when grown on GaN.

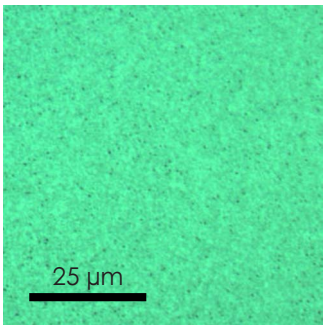

FIG. 13. (Color online) DIC optical micrograph of a 600 nm thick sample grown under growth conditions chosen from the shaded area of Fig. 2. No cracks can be observed.

The coalescence process thus causes a gradual buildup of elastic tensile strain in the growing columns despite the fact that they are lattice matched or nearly lattice matched to GaN. This gradual change of the lattice constants is what we observe in our XRD measurements. The tensile strain can be relaxed only if a sufficient number of adatoms is reaching the grain boundaries. However, at the employed low temperature and high N flux, the adatom mobility is low and the incoming atoms are incorporated very close to their arrival point. The tensile strain increases and at a certain thickness it becomes so high that the layer cracks.

D. Growth of crack-free (Al,In)N layers

The tensile stresses resulting from the crystallite coalescence process can be relaxed through incorporation of additional adatoms at the grain boundaries that are forming. Therefore, the surface diffusion length of the arriving atoms must be large enough to allow the atoms to reach the grain boundaries. This can be achieved by increasing the growth temperature, decreasing the N flux, and decreasing the growth rate. These actions are, however, limited to a very narrow window since an increase of the adatom mobility promotes phase separation. Indeed, samples exhibit phase separation and InN crystallite formation already at a growth temperature as low as 450 °C. The metal-rich growth conditions that are commonly used for the growth of many nitrides to increase the adatom mobility cannot be used here because they give rise to metal inclusions in the layer and, eventually, they lead to a transition to polycrystalline growth. We obtained homogeneous and crack-free layers with a thickness of 600 nm by using the growth conditions from the shaded area in Fig. 2 (using a growth rate of ≈200 nm/h).

Figure 13 shows a DIC optical micrograph from the surface of a crack-free 600 nm thick $Al_{0.8}In_{0.2}N$ sample grown at 400 °C with an N flux of 1 sccm. An ω-2θ XRD scan of this sample is shown in Fig. 14. We achieve a good agreement between simulation and experimental data without including a strain gradient. Figure 15 displays the corresponding RSM for this sample. The contour plot shows that there is only one reflection related to the (Al,In)N film in contrast to the two (Al,In)N peaks visible in the RSM obtained from

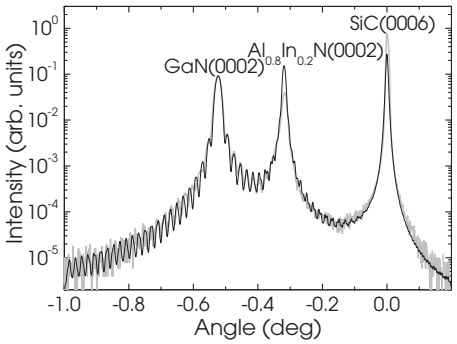

FIG. 14. XRD ω-2θ scan across the GaN(0002) reflection of the sample shown in Fig. 13. No strain gradient was needed to fit (black line) the experimental data (gray line).

the sample grown under nonoptimized conditions (Fig. 8). In Fig. 15 the $Al_{0.8}In_{0.2}N$ reflection lies to the left of the GaN reflection (marked by the white dashed line in the figure) which means that a of this (Al,In)N layer is larger than that of GaN. This is consistent with the In content of 20% which is 3% more than the 17% required for obtaining lattice-matched conditions.

IV. GROWTH OF (Al,In)N/GaN MULTILAYERS

A. Growth conditions

We were able to grow lattice-matched and therefore crack-free $Al_{0.82}In_{0.18}N/GaN$ multilayers by employing growth conditions found in the shaded region in Fig. 2. As mentioned, these growth conditions correspond to the optimum growth conditions for our (Al,In)N layers. The $Al_{0.82}In_{0.18}N$ layers were grown at 400 °C with a N flux of 1 sccm yielding N-rich growth conditions with a growth rate of $\Gamma_{(Al,In)N}=200$ nm/h. The Al and In shutters were closed and the growth temperature was ramped to 650 °C prior to the growth of the GaN layers. The N flux was kept at 1 sccm

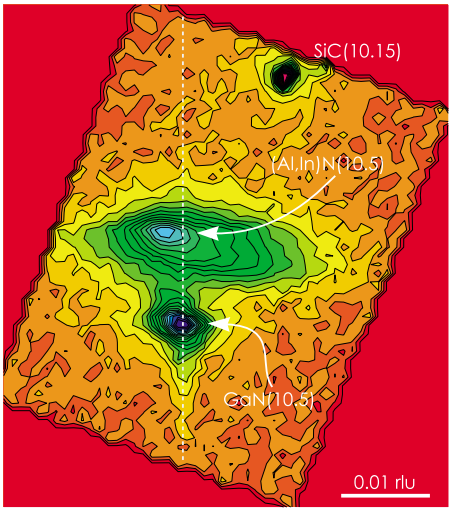

FIG. 15. (Color online) Reciprocal space map of the sample shown in Fig. 13. Indicated are the reflections corresponding to the SiC substrate, the GaN buffer layer, and the $Al_{0.8}In_{0.2}N$ film.

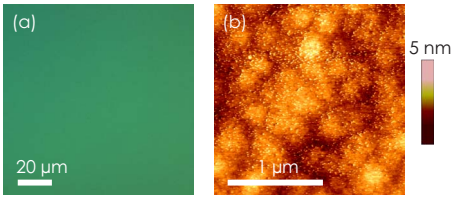

FIG. 16. (Color online) (a) DIC optical micrograph of the surface of a sample consisting of 11 periods of $Al_{0.82}In_{0.18}N/GaN$. No cracks are observed. (b) AFM micrograph of the surface of this sample. The small bright dots interspersed over the surface are the individual columns. Peak-to-valley and rms roughnesses are 5.2 and 0.53 nm, respectively.

which in this case gave Ga-stable growth conditions with a growth rate of $\Gamma_{GaN}=400$ nm/h. At the end of the GaN layers the growth temperature was again ramped down to 400 °C before the start of the next $Al_{0.82}In_{0.18}N$ layer.

A RHEED pattern indicating shallow (<5°) facets on the growth front was observed during the growth of the $Al_{0.82}In_{0.18}N$ layers. The facet-related RHEED pattern disappeared during the growth of the GaN layers indicating a smoothening of the surface. The surface was exposed to the plasma during the temperature ramping which took 5–6 min in each direction (400→650 °C and 650→400 °C) but this did not degrade the RHEED pattern.

B. Surface, interface, and structural properties

Figure 16(a) shows a DIC optical micrograph of the surface of a 11 period $Al_{0.82}In_{0.18}/GaN$ multilayer. No cracks can be observed. In Fig. 16(b) an AFM micrograph over a 1×1 μm^2 area of the same sample is shown. The small bright dots interspersed over the surface are the individual columns. No atomic steps can be observed. The peak-to-valley and the root-mean-square (rms) roughnesses are 5.2 and 0.53 nm, respectively. These values are independent of the scan size and evidence a statistically smooth surface that is fully acceptable for optical applications.

An ω-2θ XRD scan across the GaN(0002) reflection of this sample is shown in Fig. 17. A large number of clearly resolved satellites are observed indicating a well defined periodicity and abrupt interfaces. By measuring the angular

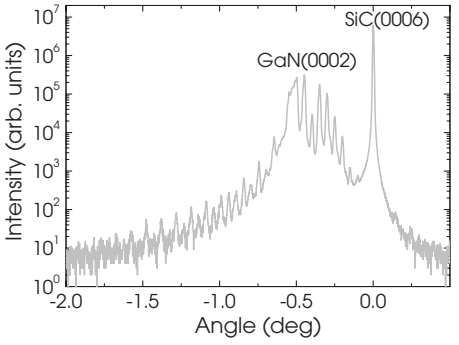

FIG. 17. XRD ω-2θ scan across the GaN(0002) reflection of the sample of Fig. 16. A large number of clearly resolved satellites are observed indicating a well defined periodicity and abrupt interfaces.

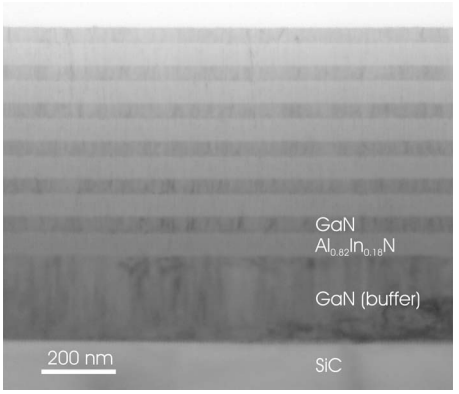

FIG. 18. Cross-sectional TEM bright-field micrograph of a six period $Al_{0.82}In_{0.18}N/GaN$ multilayer.

separation $\Delta\theta$ between the satellites we can determine the period P through

$$P = \frac{\lambda}{2\Delta\theta \cos \theta_B}, \tag{5}$$

where the λ is the wavelength of the x-rays (0.154,056,2 nm) and θ_B is the Bragg angle for GaN (17.2860°). An average $\Delta\theta$=0.049 gives a period of 94 nm.

Homogeneous and abrupt interfaces are directly visualized in Fig. 18 which shows a cross-sectional TEM bright-field micrograph of a six period $Al_{0.82}In_{0.18}N/GaN$ Bragg reflector.

C. Optical properties

The individual GaN and (Al,In)N layer thicknesses of the 6 and 11 period samples have been chosen to correspond to the $\lambda/4$ thicknesses of Bragg reflectors with stop bands at 550 and 450 nm, respectively. Reflectance measurements of these samples reveal a stop band situated very close to the desired wavelengths, but also peak reflectances as low as 0.28 for six periods and 0.38 for 11 periods. These values are significantly lower than those expected from simulations, yielding a theoretical reflectance of 0.38 and 0.75, respectively.

Since the structures exhibit smooth surfaces (Fig. 16) and abrupt interfaces (Fig. 18), interface roughness cannot be responsible for these low reflectances. We speculate that the growth conditions, while providing smooth, microscopically homogeneous, and crack-free structures, give rise to the formation of a large number of point defects and/or a preferential incorporation of In at structural defects on submicroscopic scales (particularly at the grain boundaries) resulting in strong residual absorption and scattering.

Transmittance measurements carried out for the present structures remained inconclusive due to the absorption of doped SiC substrates in the visible spectral range. Thus, the transmittance measurements have to be done using structures grown on truly transparent substrates. Furthermore, attempts to detect a possible agglomeration of In using EELS were unsuccessful; the layers appear to be homogeneous down to the smallest length scale accessible to us (100 nm).

V. CONCLUSION

One of the advantages with PAMBE compared to other epitaxial growth techniques is the possibility to impose kinetic restrictions by lowering the growth temperature while sustaining a high quality of the grown layers. Growth at 400 °C with gas-source MBE or MOCVD is virtually impossible because of the extremely low cracking efficiency of ammonia at this low temperature. For example, the growth of both In- and N-phase InN is dominated by PAMBE since this binary requires a relatively low growth temperature.

It was therefore expected at the beginning of this (Al,In)N growth study that PAMBE would be the preferred growth method. However, as we have seen in the course of this work, the low adatom mobility at the low growth temperatures employed gave rise to crystallite coalescence and grain-boundary formation. This effect introduces a tensile stress in $Al_{0.82}In_{0.18}N$ films despite the fact that $Al_{0.82}In_{0.18}N$ is lattice matched to GaN. The tensile stress increases with the layer thickness and at a certain thickness the stress becomes so high that the layer cracks. The stress can be relaxed by increasing the adatom mobility which can be achieved by increasing the growth temperature, decreasing the N flux, and decreasing the growth rate. All these proposed actions are limited to a very narrow range since an increase of the adatom mobility promotes phase separation. Phase separation and InN crystallite formation was seen in samples grown at a temperature as low as 450 °C.

Based on our growth experiments we have constructed a phase diagram which helped us identify a very narrow but viable growth window for growing crack-free (Al,In)N layers. A growth temperature of 400 °C yielded homogeneous and crack-free films with smooth surfaces. These conditions were employed to grow lattice-matched $Al_{0.82}In_{0.18}N/GaN$ multilayers which were crack free and exhibited smooth surface morphologies and abrupt interfaces. The observed reflectance of 0.4 is much lower than the expected reflectance of $>$0.7. The cause for this finding might be residual absorption by point defects and/or scattering by In rich regions on a submicroscopic scale. Further work is required to determine the actual origin of this phenomenon and to identify possible remedies.

ACKNOWLEDGMENTS

We would like to thank Hans-Peter Schönherr, Michael Höricke, and Claudia Hermann for their invaluable technical assistance. Further, we are indebted to Daniel Schaadt for his help with the AFM and the RSM image processing.

*Present address: Materials Research Laboratory, University of California, Santa Barbara, California 93106-5121, USA: ive@ece.ucsb.edu

†Present address: Department of Physics and Astronomy, Kelvin Building, University of Glasgow, G12 8QQ, Scotland, United Kingdom.

[1] I-hsiu Ho and G. B. Stringfellow, Appl. Phys. Lett. **69**, 2701 (1996).
[2] T. Matsuoka, Appl. Phys. Lett. **71**, 105 (1997).
[3] J.-F. Carlin and M. Ilegems, Appl. Phys. Lett. **83**, 668 (2003).
[4] J.-F. Carlin, J. Dorsaz, E. Feltin, R. Butté, N. Grandjean, M. Ilegems, and M. Laügt, Appl. Phys. Lett. **86**, 031107 (2005).
[5] J. Dorsaz, J.-F. Carlin, S. Gradecak, and M. Ilegems, J. Appl. Phys. **97**, 084505 (2005).
[6] J. Dorsaz, H.-J. Bühlmann, J.-F. Carlin, N. Grandjean, and M. Ilegems, Appl. Phys. Lett. **87**, 072102 (2005).
[7] J. Kuzmik, IEEE Electron Device Lett. **22**, 510 (2001).
[8] A. Dadgar, F. Schulze, J. Bläsing, A. Diez, A. Krost, M. Neuburger, E. Kohn, I. Daumiller, and M. Kunze, Appl. Phys. Lett. **85**, 5400 (2004).
[9] O. Katz, D. Mistele, B. Meyler, G. Bahir, and J. Salzman, Electron. Lett. **40**, 1304 (2004).
[10] M. Higashiwaki and T. Matsui, Jpn. J. Appl. Phys., Part 2 **43**, L768 (2004).
[11] S. Yamaguchi, R. Izaki, N. Kaiwa, S. Sugimura, and A. Yamamoto, Appl. Phys. Lett. **84**, 5344 (2004).
[12] T. Seppänen, P. O. A. Persson, L. Hultman, J. Birch, and G. Z. Radnoczi, J. Appl. Phys. **97**, 083503 (2005).
[13] T. Ive, O. Brandt, H. Kostial, K. J. Friedland, L. Däweritz, and K. H. Ploog, Appl. Phys. Lett. **86**, 024106 (2005).
[14] T. Ive, O. Brandt, M. Ramsteiner, M. Giehler, H. Kostial, and K. H. Ploog, Appl. Phys. Lett. **84**, 1671 (2004).
[15] W. D. Nix and B. M. Clemens, J. Mater. Res. **14**, 3467 (1999).
[16] O. Brandt, R. Muralidharan, P. Waltereit, A. Thamm, A. Trampert, H. von Kiedrowski, and K. H. Ploog, Appl. Phys. Lett. **75**, 4019 (1999).
[17] S. W. King, C. Ronning, R. F. Davis, R. S. Busby, and R. J. Nemanich, J. Appl. Phys. **84**, 6042 (1998).
[18] C. Adelmann, J. Brault, G. Mula, B. Daudin, L. Lymperakis, and J. Neugebauer, Phys. Rev. B **67**, 165419 (2003).
[19] B. Heying, R. Averbeck, L. F. Chen, E. Haus, H. Riechert, and J. S. Speck, J. Appl. Phys. **88**, 1855 (2000).
[20] C. Adelmann, J. Brault, D. Jalabert, P. Gentile, H. Mariette, G. Mula, and B. Daudin, J. Appl. Phys. **91**, 9638 (2002).
[21] V. M. Kaganer, O. Brandt, A. Trampert, and K. H. Ploog, Phys. Rev. B **72**, 045423 (2005).
[22] O. Brandt, Y. J. Sun, H.-P. Schönherr, K. H. Ploog, P. Waltereit, S.-H. Lim, and J. S. Speck, Appl. Phys. Lett. **83**, 90 (2003).
[23] B.-T. Liou, S.-H. Yen, and Y.-K. Kuo, Appl. Phys. A **81**, 651 (2005).
[24] K. Kim, W. R. L. Lambrecht, and B. Segall, Phys. Rev. B **56**, 7018 (1997).
[25] J. E. Northrup, L. T. Romano, and J. Neugebauer, Appl. Phys. Lett. **74**, 2319 (1999).
[26] J. Chen, P. Ruterana, and G. Nouet, Phys. Rev. B **67**, 205210 (2003).